Development/Plasticity/Repair

The Stimulus-Dependent Gradient of Cyp26B1^{+} Olfactory Sensory Neurons Is Necessary for the Functional Integrity of the Olfactory Sensory Map

Hande Login, Sofia Håglin, Anna Berghard, and Staffan Bohm
Department of Molecular Biology, Umeå University, Umeå SE90187, Sweden

Stimulus-dependent expression of the retinoic acid-inactivating enzyme Cyp26B1 in olfactory sensory neurons (OSNs) forms a dorsomedial (DM)–ventrolateral (VL) gradient in the mouse olfactory epithelium. The gradient correlates spatially with different rates of OSN turnover, as well as the functional organization of the olfactory sensory map, into overlapping zones of OSNs that express different odorant receptors (ORs). Here, we analyze transgenic mice that, instead of a stimulus-dependent Cyp26B1 gradient, have constitutive Cyp26B1 levels in all OSNs. Starting postnatally, OSN differentiation is decreased and progenitor proliferation is increased. Initially, these effects are selective to the VL-most zone and correlate with reduced ATF5 expression and accumulation of OSNs that do not express ORs. Transcription factor ATF5 is known to stabilize OR gene choice via onset of the stimulus-transducing enzyme adenylyl cyclase type 3. During further postnatal development of Cyp26B1 mice, an anomalous DM^{high}–VL^{low} expression gradient of adenylyl cyclase type 3 appears, which coincides with altered OR frequencies and OR zones. All OR zones expand ventrolaterally except for the VL-most zone, which contracts. The expansion results in an increased zonal overlap that is also evident in the innervation pattern of OSN axon terminals in olfactory bulbs. These findings together identify a mechanism by which postnatal sensory-stimulated vitamin A metabolism modifies the generation of spatially specified neurons and their precise topographic connectivity. The distributed patterns of vitamin A-metabolizing enzymes in the nervous system suggest the possibility that the mechanism may also regulate neuroplasticity in circuits other than the olfactory sensory map.

Key words: **activity dependent; odorant receptors; olfactory sensory neurons; retinoic acid; sensory map; vitamin A**

Significance Statement

The mouse olfactory sensory map is functionally wired according to precise axonal projections of spatially organized classes of olfactory sensory neurons in the nose. The genetically controlled mechanisms that regulate the development of the olfactory sensory map are beginning to be elucidated. Little is known about mechanisms by which sensory stimuli shape the organization of the map after birth. We show that a stimulus-dependent gradient of a retinoic acid-inactivating enzyme Cyp26B1 modifies the composition, localization, and axonal projections of olfactory sensory neuron classes. The mechanism is novel and suggests the interesting possibility that local vitamin A metabolism could also be a mediator of stimulus-dependent modifications of precise spatial connectivity in other parts of the nervous system.

Introduction

Sensory maps are formed by spatially organized classes of peripheral sensory cells and orderly axon projections to target neurons in the brain and are typically composed of various unique entities (or subsystems) that fulfill different functions in stimulus detection or coding. One such example is the odorant receptor (OR) zones in the mouse that are formed by spatial restrictions of more than a thousand different classes of olfactory sensory neurons (OSNs), each expressing a defined OR (Buck and Axel, 1991; Ressler et al., 1994; Vassar et al., 1994; Nishizumi and Sakano, 2015). ORs are G-protein-coupled receptors that signal the presence of odorants via type III adenylyl cyclase (AC3)-mediated

Received June 11, 2015; revised Aug. 31, 2015; accepted Sept. 5, 2015.

Author contributions: H.L., S.H., A.B., and S.B. designed research; H.L., S.H., A.B., and S.B. performed research; S.B. contributed unpublished reagents/analytic tools; H.L., S.H., A.B., and S.B. analyzed data; S.B. wrote the paper.

This work was supported by the Swedish Medical Science Research Council (Grant K2008-63X-20726-01-3). We thank Viktoria Vedin for expert advice on immunohistochemistry, Peter Mombaerts for the P2-IRES-tauLacZ mouse line, Jörg Strotmann for the MOL2.3-IRES-tauLacZ mouse line, and Sara Wilson and Devendra Maurya for critical reading of the manuscript.

The authors declare no competing financial interests.

Correspondence should be addressed to Staffan Bohm, Department of Molecular Biology, Umeå University, Umeå SE90187, Sweden. E-mail: Staffan.Bohm@umu.se.

DOI:10.1523/JNEUROSCI.2247-15.2015

 0270-6474/15/3513807-12$15.00/0

cAMP production and opening of cyclic nucleotide-gated (CNG) ion channels. OSNs, expressing different ORs, are organized in overlapping zones along the dorsomedial (DM)–ventrolateral (VL) axis of the olfactory epithelium. This organization determines the dorsal/ventral positioning of glomeruli in the olfactory bulb (Ressler et al., 1994; Vassar et al., 1994; Nishizumi and Sakano, 2015). Glomeruli are spherical structures in which synapses between OSNs and target neurons are formed. Recent studies indicate that OSNs in the DM olfactory epithelium can mediate innate aversive and social behaviors in response to odorants, whereas both DM and VL OSNs can mediate conditional behaviors to odorants (Kobayakawa et al., 2007; Jones et al., 2008; Cho et al., 2011; Ferrero et al., 2011; Dewan et al., 2013; Li et al., 2013; Dias and Ressler, 2014; Matsuo et al., 2015). The turnover of VL OSNs is higher than that of DM OSNs (Vedin et al., 2009). This spatial asymmetry in neurogenesis develops after the first postnatal week. Odorants increase the longevity of OSNs and one function of postnatal OSN turnover is cell selection that shapes the repertoire of OR-specific OSN classes to a changing odor environment (Santoro and Dulac, 2012). The numbers of OSNs expressing defined ORs also change in response to sensory deprivation by naris closure (Zhao et al., 2013) and after conditioned learning (Jones et al., 2008; Dias and Ressler, 2014).

Cytochrome P450, family 26, subfamily B, polypeptide 1 (Cyp26B1) is an enzyme that inactivates the diffusible vitamin A metabolite all-*trans* retinoic acid (RA), which regulates gene expression through nuclear RA receptors (RARs) (Ross and Zolfaghari, 2011). Cyp26B1 is expressed in OSNs in a stimulus- and CNG-channel-dependent manner (Öztokatli et al., 2012; Login et al., 2015). Cyp26B1$^+$ OSNs form a DM^{high}–VL^{low} gradient in the postnatal olfactory epithelium that correlates with the DM–VL organization of the OR expression zones (Login et al., 2015). In addition to Cyp26 enzymes, tissue levels of RA are controlled by RA-synthesizing retinaldehyde dehydrogenases (RALDHs). In the olfactory epithelium, RALDHs are expressed in non-neural cells located predominantly in the VL olfactory epithelium and lamina propria (Norlin et al., 2001; Niederreither et al., 2002; Asson-Batres and Smith, 2006; Peluso et al., 2012). RA regulates OSN progenitor cell fate during embryonic development (LaMantia et al., 2000; Paschaki et al., 2013). In postnatal and adult mice, RAR-dependent expression has been shown to promote survival of OSNs (Hägglund et al., 2006), maintenance of OR-specific glomeruli (Öztokatli et al., 2012), and OSN recovery after trauma (Peluso et al., 2012).

Here, we analyze mice in which the activity-dependent Cyp26B1 gradient in the olfactory epithelium is disrupted. Surprisingly, constitutive Cyp26B1 expression in all zones leads to the appearance of a DM^{high}–VL^{low} gradient of AC3, together with decreases in ATF5$^+$ and OR$^+$ OSNs in the VL epithelium. In the DM epithelium, the expression of individual OR genes increases or is unaltered. The zonal distribution in the epithelium, and the corresponding glomerular distribution in the olfactory bulb, both expand in the VL direction. These results indicate that the mechanisms underlying neurogenesis and OR gene choice progressively show increased sensitivity to changes in RA bioavailability along the DM–VL epithelial axis. Stimulus-dependent Cyp26B1 expression in the DM olfactory epithelium can thus function as an "RA sink" that contributes to maintaining OSN classes mediating innate behaviors and at the same time stimulating turnover and adaptation of more ventrolaterally located OSNs.

Materials and Methods

Tissue preparation. OMP-Cyp26B1 mouse lines were generated by ligating the coding sequence of Cyp26B1 (bp 360-1931 of NM_175475) 3′ to the mouse olfactory marker protein (OMP) gene promoter and 5′ to a simian virus 40 (SV40) polyadenylation site as described previously (Login et al., 2015). Two independent founder lines expressing Cyp26B1 selectively in OSNs were backcrossed to C57BL/6J mice (Taconic) for > 4 generations and hemizygous mice of either sex were analyzed. Results obtained with progeny from both founder lines were similar (data not shown). Phenotype characterization was performed using the F1 generations from crosses between OMP-Cyp26B1 transgenic mice and OR-reporter mice in a C57BL/6 genetic background. OR-reporter mice were; P2-IRES-tauLacZ (Mombaerts et al., 1996) and MOL2.3-IRES-tauLacZ (Conzelmann et al., 2000). Immediately after cervical dislocation, the mice were exsanguinated and tissue was dissected, fixed for 3 h at 4°C in 4% (w/v) paraformaldehyde in PBS, pH 7.4, cryoprotected in 20% (w/v) sucrose at 4°C for 16–24 h, frozen in Tissue-Tek optimal cutting temperature medium (Sakura Finetek), and cryosectioned at 10 μm. Tissue from >3-week-old mice was treated with RDO Rapid Decalcifier before cryoprotection (ApexEngineering). All animal experiments were approved by the local ethics committee for animal research at the court of appeal for the upper northern area of Norrland (Umeå, Sweden).

In situ *hybridization.* Digoxygenin-labeled cRNA probes specific for RALDH3, MOR40-14, MOR244-1 (MOR28), and MOR265-3 (P2) were generated from EST clones with GenBank Accession No. AA790530, BC104299, NM_001170918, and BC139721, respectively. The MOR35-1-specific probe was generated from cloned cDNA corresponding to bp 101–770 of GenBank Accession No. BC132004. Sense probes did not generate hybridization signals above background. Probes for Cyp26B1, RALDH1, RALDH2, MOR161-6 (K21), MOR235-1 (A16), MOR256-55 (L45), and MOR256-17 were as described previously (Norlin et al., 2001; Oztokatli et al., 2012). For the *in situ* hybridization protocol used (Ishii et al., 2004), which includes a posthybridization step with RNaseA, it has been reported that there is no risk for cross-hybridization if the sequence identity between ORs is <80% (Ishii et al., 2004). Sequence identities between the OR probes used in this study and their most closely related OR family member were; 76% (MOR40-14), 84% (MOR161-6), 75% (MOR263-5), 73% (MOR35-1), 67% (MOR256-17), 82% (MOR256-55), 72% (MOR235-1), and 85% (MOR244-1)."

Immunohistochemistry. Background was blocked by incubation for 1 h in 3% normal donkey serum in PBS with 0.1% Triton X-100, followed by overnight incubation at 4°C in blocking solution containing anti-NQO1 (dilution 1:500; catalog #ab2346; Abcam), anti-NCAM2 (1:200; catalog #AS05 077; Agrisera), anti-Cyp26B1 (1:200; catalog #21555-1-AP; ProteinTech), anti-β-galactosidase (1:1000; catalog #559762, MP-Cappel), anti-AC3 (1:500; catalog #C-20; Santa Cruz Biotechnology), anti-cleaved caspase 3 (1:500; catalog #559565; BD Biosciences), anti-phospho-histone 3 (pH3, 1:500; catalog #06-570; Millipore), anti-OMP (1:1000; catalog #544-10001; Wako Chemicals), and anti-SCG10 (Stathmin-1; 1:500, catalog #AS02024; Agrisera). After washes, specific fluorescent immunostaining was visualized after incubation 1 h at room temperature with Alexa Fluor 488/546-conjugated anti-goat IgG or Alexa Fluor 488/546-conjugated anti-rabbit IgG (1:1000; Invitrogen). Alternatively, tissue sections were incubated with biotinylated anti-rabbit IgG (1:500; Invitrogen) or biotinylated anti-goat IgG (1:1000; Invitrogen), followed by avidin-conjugated horseradish peroxidase (Vector Laboratories) and 3,3′-diaminobenzidine as a substrate. Sections were counterstained with Hoechst 33258 (Sigma-Aldrich). Images of double immunohistochemical analyses were produced using a Nikon Digital Eclipse C1 plus confocal microscope. For β-galactosidase (β-gal) histochemical staining, 10 μm tissue sections of P2 and MOL2.3 reporter mice were rinsed in 0.1 M phosphate buffer, 2 mM $MgCl_2$, 5 mM EGTA, 0.02% Nonidet-P40, and 0.001% sodium deoxycholate and stained in buffer with 1 mg/ml 5-bromo-4-chloro-3-indolyl-β-D-galactopyranoside, 5 mM $K_3Fe(CN)_6$, and 5 mM $K_4Fe(CN)_6$ overnight at 37°C. Sections were rinsed in PBS and counterstained with Hoechst 33258.

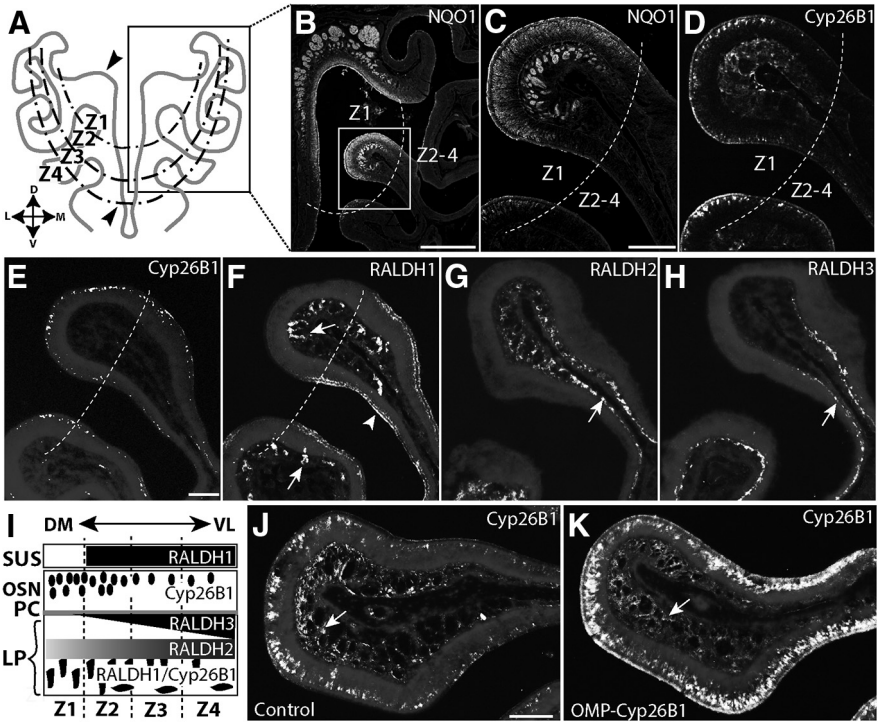

Figure 1. Expression of Cyp26B1 and RALDH isoforms in the olfactory mucosa. ***A***, Drawing of the olfactory epithelium in coronal plane is shown. Z1-4 (boundary markers) are indicated, as are the epithelial regions that was analyzed in experiments shown in Figures 3*C* and 5A-E (arrowheads). ***B–D***, Immunohistochemical analysis of consecutive sections of olfactory epithelium from PD14 mice with antibodies specific for a Z1-marker protein NQO1 (***B***, ***C***) and Cyp26B1 (***D***) is shown. ***C*** and ***D*** are enlargements of the area boxed in ***B***. Endogenous Cyp26B1 is expressed in a DM^{high}–VL^{low} gradient that crosses the Z1/Z2-4 border (dashed line). ***E–H***, *In situ* hybridization analyses of olfactory epithelium at PD14 with probes specific for Cyp26B1 (***E***), RALDH1 (***F***), RALDH2 (***G***), and RALDH3 (***H***). Sections in ***E*** and ***F*** are consecutive and the dashed line indicates a border between $RALDH1^-$ and $RALDH1^+$ sustentacular cells (arrowhead in ***F***). ***I***, Schematic illustration of Cyp26B1 and RALDH expression patterns. Sus, Sustentacular cells; PCs, progenitor cells; LP, lamina propria. High expression is indicated by black. Scattered $Cyp26B1^+$ OSNs form a DM^{high}–VL^{low} gradient in the olfactory epithelium, which is inverse to the overall DM^{low}–VL^{high} distribution of RALDH expression. Previous studies have shown that RALDH1, in addition to sustentacular cells, is expressed in ensheathing cells and gland cells (***F***, arrows), whereas RALDH2 and RALDH3, respectively, are expressed in lamina propria fibroblasts (arrow in ***G***) and in cells directly subjacent to the basal lamina (arrow in ***H***; Asson-Batres and Smith, 2006; Peluso et al., 2012). Consistent with a previous study, Cyp26B1 is also expressed in cells of lamina propria (arrows in ***J*** and ***K***) that, like RALDH1 mRNA expression in lamina propria, appears patchy, but cells are equally distributed along the DM–VL extent of the nasal cavity (Login et al., 2015). ***J***, ***K***, Cyp26B1 immunohistochemical analysis of 5-week-old control (***J***) and littermate Cyp26B1 transgenic (***K***) mice. Cyp26B1 is overexpressed in the olfactory epithelium, but not in the lamina propria in transgenic mice (arrows). Scale bars: ***B***, 500 μm; ***C–H***, ***J***, ***K***, 100 μm.

Data analysis. At least three pairs of control and transgenic littermate mice were analyzed for each condition. All averaged data are presented as mean ± SD per hemisection of the olfactory epithelium or bulb. The measurement of linear length of olfactory epithelium in PD45 mice was done on sections collected from middle and posterior regions of the olfactory epithelium, eight sections from each region and mouse (section interval 48 μm). Immunoreactive areas were quantified using confocal images of 100-μm-long olfactory epithelial regions with NIS elements AR (Nikon) software. NQO1 immunohistochemical staining was used as a marker for Z1. Both AC3 immunohistochemical staining and the olfactory–respiratory epithelial border were used as markers for the length of olfactory epithelium. The length of NQO1- and NCAM2-immunoreactive regions were measured in the glomerular layer and related to the total circumference of the olfactory bulb. Data were obtained from eight hemisections per mouse (section interval 90 μm). Quantifications of cells staining positive for activated caspase-3, pH 3, Hoechst, and ORs were performed in eight sections (section interval 90 μm) collected from the middle part of the olfactory epithelium. The sections had characteristic morphology as shown in Figure 1*A*. Consecutive sections from each animal were analyzed with different OR probes, as well as with anti-activated caspase-3 and anti-pH3 antibodies. Immunohistochemistry data for Z1 and Z4 were obtained from the DM and VL regions indicated with arrowheads shown in Figure 1*A*. Measurement of cell size of Z1 and Z4 OSNs showed that the diameter of Z1 OSNs was 5.76 ± 0.07 and 5.59 ± 0.10 μm in control and transgenic mice, respectively ($p = 0.31$). The corresponding numbers for Z4 OSNs were 5.72 ± 0.07 and 5.63 ± 0.1, respectively ($p = 0.50$). This result indicated that the sizes of Z1 and Z4 cell bodies were similar in control and transgenic mice and therefore that changes in immunoreactive epithelial areas most likely corresponded to changes in cell numbers and not cell sizes. Statistical significance of all datasets were determined by unpaired two-tailed *t* tests using Excel.

Results

Cyp26B1 in OSNs stimulates progenitor cell proliferation and OSN turnover

In the olfactory epithelium, each OR is expressed in a unique pattern of scattered OSNs and different ORs show overlapping spatial patterns. This organization results in numerous overlapping half concentric zones with differential OR expression rather than the originally defined four zones (Miyamichi et al., 2005). In the absence of a new terminology and for simplicity, we here use the original four zone terminology: that the most DM zone is number 1 (Z1), the most VL zone is number 4 (Z4), and two intermediate zones are Z2 and Z3 (Fig. 1*A*).

NAD(P)H dehydrogenase, quinone 1 (NQO1) is selectively expressed in the majority of Z1 OSNs (Fig. 1*B*,*C*; Gussing and Bohm, 2004). Immunohistochemical analyses of consecutive olfactory epithelial sections from postnatal day 14 (PD14) mice showed that the DM^{high}–VL^{low} gradient of scattered $Cyp26B1^+$ OSNs extended beyond the sharp NQO1 boundary between Z1 and Z2 and Cyp26B1 diminished further ventrolaterally (Fig. 1*D*). *In situ* hybridization experiments showed that the DM^{high}–VL^{low} gradient of the RA-inactivating enzyme Cyp26B1 was inverse to the spatial expression of the RA-producing enzymes RALDH1, RALDH2, and RALDH3 in non-neural cells of the olfactory epithelium and lamina propria (Fig. 1*E–H*). The results indicated that an OSN receives different amounts of diffusible RA depending on its relative location along the DM–VL axis of the olfactory epithelium (Fig. 1*I*). OSNs in the DM epithelium can receive the majority of RA via their axons from $RALDH2^+$ cells around axonal bundles and $RALDH1^+$ cells of the lamina propria. In more VL regions, additional $RALDH^+$ cells are present. These include $RALDH3^+$ cells close to the basal lamina and $RALDH1^+$ sustentacular cells, which constitute sources that may provide RA to immature and mature VL OSNs and VL progenitor cells close to the basal lamina. The overall spatial and cellular expression characteristics of the different RALDHs were in agreement with previous studies of RALDH mRNA expression in the olfactory mucosa (Niederreither et al., 1997; Norlin et al., 2001; Peluso et al., 2012; Login et al., 2015), as

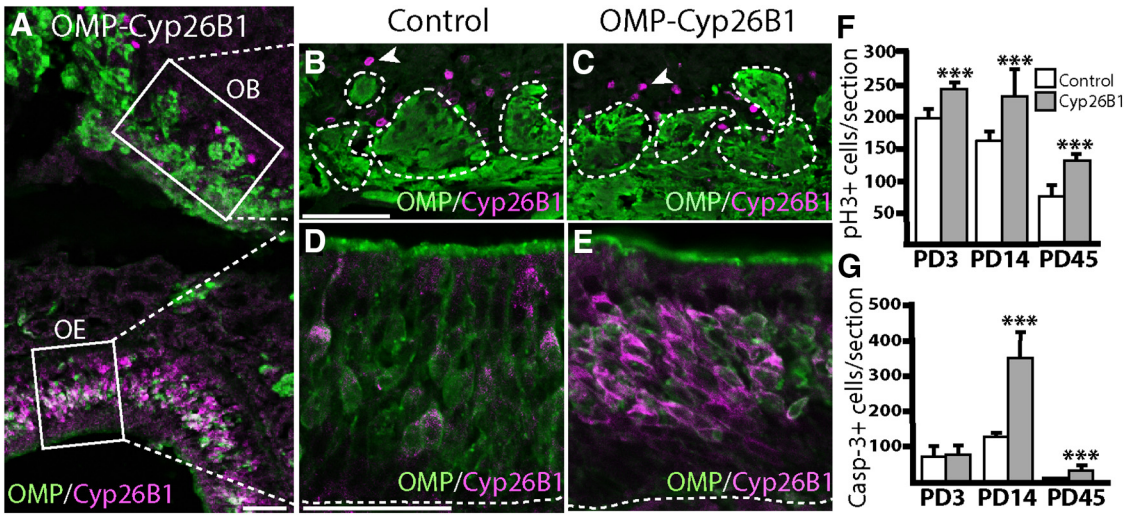

Figure 2. OMP promoter transgene-driven Cyp26B1 overexpression selectively in OSNs results in increased cell division and caspase-3 activation. ***A–E***, Double OMP (green)/Cyp26B1 (magenta) immunohistochemical analysis of the olfactory epithelia (OE) and olfactory bulbs (OBs) of a 5-week-old control mouse (***B***, ***D***) and a transgenic littermate (OMP-Cyp26B1, ***A***, ***C***, ***E***). Cyp26B1 expression is increased in OSNs and unaltered in scattered glomerular cells (arrowheads in ***B***, ***C***). Encircled in ***B*** and ***C*** are individual glomerular OMP $^{+}$ neuropils. Scale bars, 50 μm. ***F***, ***G***, Quantifications of pH3 $^{+}$ dividing cells at PD3, PD14 and PD45 (***F***) and activated caspase-3 $^{+}$ cells at PD3, PD14, and PD45 (***G***) in the olfactory epithelium of OMP-Cyp26B1 (gray bars) and littermate control mice (open bars). All values represent mean and SD per hemisection ($n = 48$), ***$p < 0.001$, Student's *t* test, two tailed.

well as spatial differences in RA-mediated transcription that has been visualized using an RA-responsive transgenic reporter mouse (Whitesides et al., 1998).

To explore the function of the activity-dependent and DM ^{high}–VL ^{low} expression of Cyp26B1 in OSNs, we analyzed transgenic mouse lines (OMP-Cyp26B1) that express Cyp26B1 under the transcriptional control of a 6 kb promoter region of the OMP gene (Login et al., 2015). The OMP promoter sequence that we used drives high constitutive transcription in OSNs, but not in their dividing progenitor cells or other cell types of the primary olfactory system (Alenius and Bohm, 2003; Hägglund et al., 2006; Öztokatli et al., 2012; Login et al., 2015). Immunohistochemical analysis showed that the normally graded Cyp26B1 expression was increased to equal high levels in OSNs throughout all OR zones in transgenic OMP-Cyp26B1 mice (Fig. 1*J*,*K*). Double Cyp26B1/OMP immunohistochemical analysis confirmed that Cyp26B1 was overexpressed in OMP $^{+}$ OSNs (Fig. 2*A*,*D*,*E*), in agreement with previous analyses (Login et al., 2015). Therefore, Cyp26B1 was overexpressed selectively in OSNs and not in other Cyp26B1 $^{+}$ cell types such as cells in lamina propria (Fig. 1*J*,*K*) or in the glomerular layer of the olfactory bulb (Fig. 2*B*,*C*).

To address the possibility that increased Cyp26B1 in postmitotic OSNs influenced OSN progenitor cell division, we performed immunohistochemical analyses and quantified the number of mitotic (pH3 $^{+}$) cells in the progenitor cell layer in transgenic Cyp26B1 mice and littermate control mice. A significant increase in mitotic cells was evident in Cyp26B1 transgenic mice during the first postnatal month (Fig. 2*F*). The numbers of dividing basal cells per section in control mice at PD3, PD14, and PD45 were; 195 ± 16, 162 ± 25, and 72 ± 17, respectively, whereas the corresponding numbers in the transgenic mice were; 240 ± 10, 230 ± 40, and 127 ± 8 ($p < 0.001$ at all time points, Student's *t* test). The number of apoptotic cells, identified by activated caspase-3 immunohistochemistry, were not significantly changed in the olfactory epithelium at PD3 (Fig. 2*G*, 74.3 ± 27 in control vs 77 ± 19 in transgenic mice, $p = 0.34$). However, during later postnatal development, the numbers of apoptotic cells were higher in OMP-Cyp26B1 transgenic mice compared with controls (Fig. 2*G*). At PD14 and PD45, the number of activated caspase-3 $^{+}$ cells per section in control mice were 138 ± 6 and 3 ± 0.6, respectively, and 359 ± 72 and 27 ± 6, respectively, in Cyp26B1 mice (control vs transgenic mice, $p < 0.001$). These results indicated that increased Cyp26B1-mediated RA degradation in postmitotic OSNs stimulated progenitor cell proliferation during the first postnatal week, whereas an increased OSN turnover—a combined increase of proliferation and OSN cell death—was not evident until the second postnatal week. Moreover, because the transgenic OMP promoter does not mediate transgenic expression in progenitor cells, the results suggested that the effect on progenitor cell division was caused by a non-cell-autonomous function of Cyp26B1, most likely inactivation of the diffusing RA produced by RALDH $^{+}$ cells.

Inverse changes of OR expression frequencies in the DM and VL olfactory epithelium

To test the hypothesis that disruption of the DM ^{high}–VL ^{low} gradient of Cyp26B1 expression affected the DM–VL organization of OR zones, OSNs expressing different zone-specific OR genes were quantified after *in situ* hybridization analyses. The expression of two ORs were analyzed after β-gal histochemistry of OSNs in the progeny of crosses between OMP-Cyp26B1 mice and OR reporter mice (MOL2.3-IRES-tauLacZ and P2-IRES-tauLac). In these reporter lines, β-gal is selectively present in OSNs expressing the Z1 OR MOR18-2 (also MOL2-3) and the Z2 OR MOR263-5 (also P2), respectively (Mombaerts et al., 1996; Conzelmann et al., 2000). Analyses of PD14 mice showed an increased number of Z1 OSNs (MOR18-2), as well as Z2 OSNs (MOR263-5 and MOR35-1) in the Cyp26B1 transgenic mice relative to littermate controls (Fig. 3*A*,*E*, Table 1). Two other Z1 OSN classes, MOR161-6 (K21) and MOR40-14, showed similar numbers in transgenic and control mice (Fig. 3*E*, Table 1). Interestingly, the numbers of OSNs expressing the Z4 ORs, MOR244-1 (also MOR28) and MOR235-1 (also A16) were significantly reduced in the transgenic mice compared with control mice (Fig. 3*C*,*E*, Table 1). The expression of an OR that defines Z3, MOR256-55 (also L45), was similar, whereas the expression

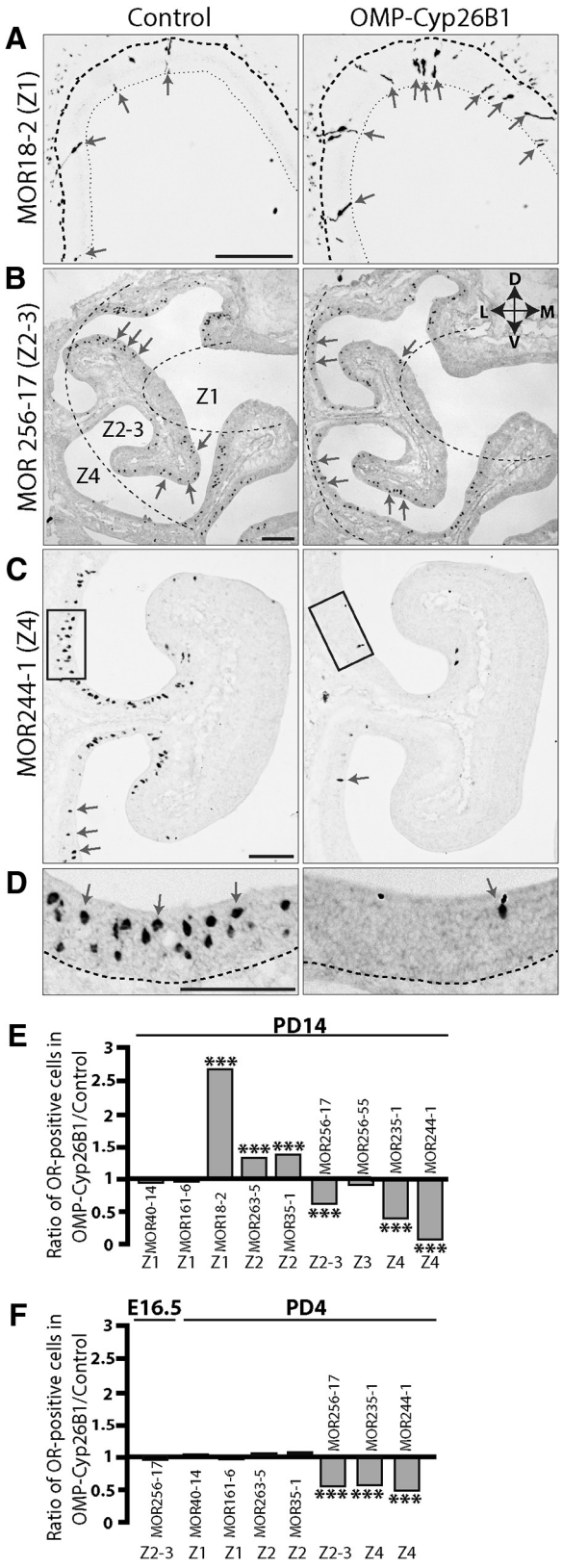

Figure 3. Disruption of the Cyp26B1 gradient affects DM and VL OR expression frequencies differently and expands zones ventrolaterally. ***A–C***, Representative images of β-gal histochemical analysis of OSNs expressing a Z1 OR (***A***) and *in situ* hybridization analysis of OSNs expressing a Z2-3 OR (***B***) and a Z4 OR (***C***) in olfactory epithelium of PD14 control and OMP-Cyp26B1 mice. Arrows indicate locations of OR$^+$ cell bodies. Dashed and dotted lines in ***A*** indicate the basal lamina and the apical surface of the olfactory epithelium, respectively. Dashed line in ***B*** indicates approximate borders for Z2-3. ***D***, Close-ups of MOR244-1 expressing cells within the epithelial regions that are boxed in ***C***. ***E***, Quantifications of the relative numbers of OSNs expressing different zone-specific ORs at PD14. Bars indicate ratio of OR$^+$ OSNs in OMP-Cyp26B1 and littermate control mice. ***F***, Quantifications of the relative numbers of OSNs expressing different zone-specific ORs at E16.5 and PD4. Bars indicate ratio of OR$^+$ OSNs in OMP-Cyp26B1 and littermate control mice. All values represent mean and SD per hemisection ($n = 48$), ***$p < 0.001$, Student's *t* test, two tailed. Scale bars, 100 μm.

of the Z2-3 OR MOR256-17 was reduced in transgenic mice (Fig. 3*B*,*E*, Table 1). Even though MOR256-17 is expressed across the Z2/Z3 boundary (Kaluza et al., 2004), the general trend was that Cyp26B1 influenced OR expression frequencies differently in the DM compared with the VL olfactory epithelium. Specifically, OR expression was increased or unaltered in Z1-2, whereas it was decreased or unaltered in Z3-4 at PD14. In Z1 and Z2, the expression frequencies of both class I and II ORs were increased or unaltered (Table 1). Class I ORs are selectively expressed in Z1 and Z2 and are phylogenetically more ancient than the class II ORs (Hirota et al., 2007).

To determine the developmental time point when the change in OR expression was first evident, OR$^+$ cells in embryonic and newborn mice were quantified. The result showed that the expression of MOR256-17 was similar in Cyp26B1 mice and littermate controls at embryonic day 16.5 (E16.5; Fig. 3*F*, Table 1). At PD4 and at PD14, the numbers of MOR256-17 (Z2-3), MOR235-1, and MOR244-1 (Z4) were reduced. However, the ORs, MOR263-5 (Z2) and MOR35.1 (Z2), which were increased at PD14, were similar to control mice at PD4 (Fig. 3*F*, Table 1). This indicated that the effect on OR expression was first evident at the first postnatal week and that the effect started in Z3-4.

Gain of Cyp26B1 function causes a postnatal VL shift of the zonal organization

A striking phenotype of the Cyp26B1 transgenic mice was that the borders of the OR zones were shifted ventrolaterally due to a DM expansion. This DM expansion was evident even for ORs that showed reduced expression frequencies, such as the Z2-3 OR MOR256-17 (Fig. 2*B*). However, no broadening was evident of the VL-most zone (Z4), which is a zone that is flanked ventrolalterally by respiratory epithelium. To quantify the VL expansion of the DM-most zone, we measured the linear epithelial length of Z1 relative to the total length of the olfactory epithelium. This was done after double NQO1/AC3 immunohistochemical staining of PD45 mice (Fig. 4*A*,*B*). NQO1 is selectively expressed in the majority of Z1 OSNs, whereas AC3 is expressed in the cilia of OSNs in all zones and not in cells of the respiratory epithelium. The average linear lengths of Z1 in control and transgenic mice were 2.7 $\pm$ 0.5 mm and 3.7 $\pm$ 0.2 mm, respectively ($p < 0.001$), whereas the total lengths in control and transgenic mice were 20.0 $\pm$ 1.4 mm and 18.2 $\pm$ 0.4 mm, respectively ($p < 0.001$). The lengths of Z1 relative to the total epithelial length were 13.5% and 20.5% in control and transgenic mice, respectively, and the total linear length of the olfactory epithelium was reduced 10% in Cyp26B1 mice. These results indicated that the ratio of Z1 versus Z2-4 zones was increased in Cyp26B1 mice and thus supported the conclusion of a postnatal DM expansion of OR zones in the transgenic mice.

Unexpectedly, from the analysis of NQO1 and AC3 expression at PD45, it became evident that the signal intensity of AC3 immunoreactivity in OSN cilia was reduced in the VL epithelium, but not in the DM epithelium, in Cyp26B1 transgenic mice (arrowhead in Fig. 4*A*). AC3 is in differentiated OSNs and stabilizes OR choice (Dalton et al., 2013). OMP is a marker protein for

←

Table 1. Changes in OR expression frequencies in control compared with Cyp26B1 mice

Zone	Class	OR gene	OR$^+$ cells		Change	Paired *t* test
			Control	OMP-Cyp26B1		
Age PD14						
Z1	I	MOR40-14	32.04 ± 1.09	30.27 ± 0.63	—	$p > 0.05$
Z1	II	MOR161-6 (K21)	31.39 ± 2.22	30.92 ± 5.62	—	$p > 0.05$
Z1	I	MOR18-2 (MOL2.3)*	4.61 ± 1.34	13.19 ± 1.47	↑	$p < 0.001$
Z2	II	MOR263-5 (P2)*	39.69 ± 9.07	57.33 ± 12.41	↑	$p < 0.001$
Z2	I	MOR35-1	34.14 ± 4.24	47.72 ± 4.84	↑	$p < 0.001$
Z2-3	II	MOR256-17	208.13 ± 12.88	124.75 ± 12.17	↓	$p < 0.001$
Z3	II	MOR256-55 (L45)	73.24 ± 9.16	70.21 ± 5.80	—	$p > 0.05$
Z4	II	MOR235-1 (A16)	111.26 ± 9.38	50.12 ± 7.24	↓	$p < 0.001$
Z4	II	MOR244-1 (MOR28)	117.28 ± 5.12	16.27 ± 3.91	↓	$p < 0.001$
Age E16.5						
Z2-3	II	MOR256-17	31.067 ± 1.16	29.39 ± 0.77	—	$p > 0.05$
Age PD4						
Z1	I	MOR40-14	4.29 ± 0.26	4.39 ± 0.92	—	$p > 0.05$
Z1	II	MOR161-6 (K21)	3.88 ± 0.39	3.57 ± 0.17	—	$p > 0.05$
Z2	II	MOR263-5 (P2)	7.21 ± 1.12	7.72 ± 0.74	—	$p > 0.05$
Z2	I	MOR35-1	26.77 ± 8.19	29.67 ± 2.89	—	$p > 0.05$
Z2-3	II	MOR256-17	86.08 ± 14.51	47.50 ± 11.06	↓	$p < 0.001$
Z4	II	MOR235-1 (A16)	33.29 ± 1.23	18.38 ± 0.67	↓	$p < 0.001$
Z4	II	MOR244-1 (MOR28)	53.7 ± 13.74	26.14 ± 8.53	↓	$p < 0.001$

OR expression frequencies are presented as mean OR$^+$ cells ± SD per hemisection ($n = 48$), Student´s *t* test, two tailed. Similar frequencies in control and Cyp26B1 mice are indicated with —; higher and lower frequencies in Cyp26B1 mice compared with control mice are indicated with ↑ and ↓, respectively.

*βgal$^+$ cells quantified in heterozygous OR-reporter mice.

differentiated OSNs. Double AC3/OMP immunohistochemical analysis showed that the reduction in AC3 expression in the VL olfactory epithelium correlated with reduced OMP expression in Cyp26B1 mice (Fig. 4*C*). This result was consistent with the idea that increased Cyp26B1 expression resulted in fewer mature OSNs in the VL olfactory epithelium at PD45. Remarkably, the intensity of AC3 immunoreactivity decreased gradually ventrolaterally (Fig. 4*A*). Collectively, these results indicated that the disruption of the DM^{high}–VL^{low} Cyp26B1 expression gradient in the Cyp26B1 transgenic mice gave rise to an aberrant DM^{high}–VL^{low} gradient of OSN differentiation. We next performed double pH3/NQO1 analysis of the olfactory epithelium to determine whether there were differences in the number of dividing basal progenitor cells at PD45 in Z1 and Z2-4 of control versus transgenic mice (Fig. 4*D*). The number of dividing cells in Z1 of control and transgenic mice were 0.9 ± 0.1/mm and 1.5 ± 0.2/mm, respectively ($p < 0.001$). The number of dividing cells in Z2-4 of control and transgenic mice were 1.7 ± 0.3/mm and 4.0 ± 0.1/mm, respectively ($p < 0.001$). Therefore, increasing RA inactivation in OSNs stimulated progenitor cell proliferation 1.5-fold in Z1 and 2.4-fold in Z2-4 at PD45.

Expanded innervation by DM OSNs into the ventral olfactory bulb

The zonal organization is maintained in the axon projections of OSNs to the olfactory bulb; that is, projections from different zones terminate in separate glomerular regions that are organized in a dorsal–ventral manner in the olfactory bulb (Astic and Saucier, 1986; Saucier and Astic, 1986; Ressler et al., 1994; Vassar et al., 1994; Alenius and Bohm, 1997; Gussing and Bohm, 2004; Miyamichi et al., 2005). To analyze whether the altered Cyp26B1 expression also had consequences for the dorsal–ventral zonal organization of glomeruli, we quantified the relative distribution of NQO1 and NCAM2 (also RNCAM/OCAM) immunoreactivity in the glomerular layer of PD45 mice (Fig. 5*A*–*E*). NQO1 and NCAM2 are selectively expressed in axons of Z1 and Z2-4 OSNs, respectively (Alenius and Bohm, 1997; Yoshihara et al., 1997; Gussing and Bohm, 2004). The analysis demonstrated that circumferences of the glomerular layer in control and OMP-Cyp26B1 mice were similar (4.7 ± 0.35 mm and 4.6 ± 0.35 mm). The lengths of the NQO1$^+$ (Z1) glomerular layer in control and Cyp26B1 transgenic mice were 2.5 ± 0.4 mm and 3.2 ± 0.3 mm, respectively ($p < 0.001$). The lengths of the NCAM2$^+$ (Z2-4) glomerular layer in control and Cyp26B1 transgenic mice were 2.2 ± 0.5 mm and 1.8 ± 0.5 mm, respectively ($p < 0.05$). In agreement with the increased olfactory epithelial Z1 in Cyp26B1 mice, these results showed that that the Z1 glomerular layer was increased 15%, whereas the Z2-4 glomerular layer was decreased 7% in transgenic mice relative to control mice (Fig. 5*A*–*C*). These data indicated that high constitutive expression of Cyp26B1 during the first ~1.5 months of postnatal life resulted in a relative expansion of the DM glomerular area at the expense of a diminished VL glomerular area. Moreover, by subtracting the total length of the glomerular layer from the combined length of NQO1$^-$ and NCAM2$^+$ glomerular layer, it was evident that 8% of the glomerular layer in Cyp26B1 transgenic mice was innervated by both NQO1$^+$ and NCAM2$^+$ axon terminals (Fig. 5*C*). In agreement with this finding, an increased number of glomeruli that received heterogeneous innervation of both NQO1$^+$ and NCAM2$^+$ axon terminals were located ventral to the border between NCAM2$^-$ and NCAM2$^+$ glomeruli in Cyp26B1 transgenic mice (Fig. 5*D*,*E*). This indicated that the expansion of the DM glomerular area was a consequence of DM OSN axons spreading and co-innervating more ventrally located glomeruli.

To address whether increased Cyp26B1 expression in OSNs resulted in an increased number of OR-specific glomeruli and/or the formation of heterogeneous glomeruli incorrectly innervated by axons of >1 OR identity, we analyzed transgenic mice bred to MOL2.3-IRES-tauLacZ and P2-IRES-tauLacZ reporter mice. In these mice, β-gal is present in the axons of OSNs that express the ORs MOR18-2 and MOR263-5, respectively. MOR18-2 is a Z1 OR and MOR263-5 is a Z2 OR, which both showed increased OSN numbers in the Cyp26B1 mice (Fig. 3*E*). OMP immunoreactivity and β-gal histochemical staining overlap throughout a glomerulus ho-

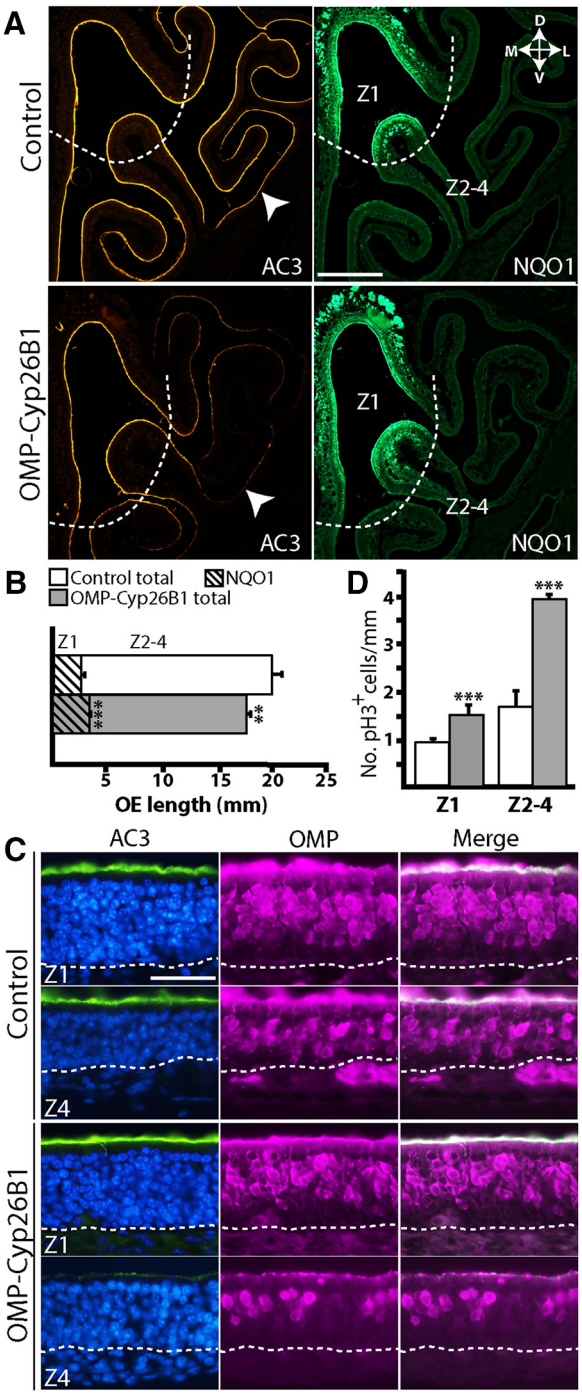

Figure 4. Increased Cyp26B1 expression results in an expanded Z1 and the formation of a DM^{high}–VL^{high} gradient of AC3 expression ***A***, Representative images of double AC3 (yellow) and NQO1 (green) immunohistochemical analyses of olfactory epithelium in Cyp26B1 and control mice at PD45. Dashed lines represent the border between Z1 and Z2-4 identified by NQO1 immunoreactivity. Arrowheads indicate reduced AC3 expression in the cilia of OSNs in the VL olfactory epithelium of a transgenic mouse. In Cyp26B1 mice, AC3 is expressed in a DM^{high}–VL^{low} gradient, whereas, in control mice, AC3 is expressed at an equal level in cilia throughout the olfactory epithelium. ***B***, Quantification of relative linear lengths of the olfactory epithelium and Z1 (striped) in Cyp26B1 transgenic mice (gray bars) and littermate control mice (open bars) at PD45. ***C***, Representative images of double AC3 (green) and OMP (magenta) immunohistochemical analyses of DM and VL regions of olfactory epithelium of PD45 Cyp26B1 mice and littermate control mice. ***D***, Quantifications of $pH3^+$ dividing cells in Z1 and Z2-4 regions in the olfactory epithelium of PD45 Cyp26B1 mice (gray bars) and littermate control mice (open bars). All values represent mean and SD per hemisection ($n = 48$), $^{**}p < 0.01$, $^{***}p < 0.001$, Student's *t* test, two tailed. Scale bars: ***A***, 400 μm; ***D***, 50 μm.

mogeneously innervated by axons of one OR identity (Zou et al., 2004; Öztokatli et al., 2012; Fig. 5*F*). In contrast, a heterogeneous glomerulus with axons of >1 OR identity contains an OMP^+ neuropil divided into β-gal^+ and β-gal^- domains, in which the latter correspond to axons of OSN classes expressing other ORs than the OR reporter gene (Fig. 5*F*). Double β-gal/OMP immunohistochemistry of serial coronal sections through the olfactory bulbs of PD45 mice revealed that the Cyp26B1 transgenic mice had an increased total number of MOR18-2 glomeruli (1.3 ± 0.3 glomeruli/half-bulb in controls vs 2.2 ± 0 in transgenic mice, $p < 0.01$) and MOR263-5 glomeruli (1.3 ± 0.3 glomeruli/half-bulb in controls mice vs 2.5 ± 0.2 in transgenic mice, $p < 0.01$). All MOR18-2 and MOR263-5 glomeruli were homogeneous in control mice, whereas the majority was heterogeneous in Cyp26B1 transgenic mice (Fig. 5*G*). OSNs expressing the same OR form at least one glomerulus located on both the medial and lateral aspect of each bulb (Ressler et al., 1994; Vassar et al., 1994), which gives rise to a mirror-symmetric glomerular maps in each bulb. Analyses of the location of the supernumerary ectopic glomeruli in Cyp26B1 mice showed that these additional glomeruli were located ventral relative to the locations of homogeneous MOR18-2 and MOR263-5 glomeruli (Fig. 5*H*). Together, these results indicated that the DM zonal expansion in the olfactory epithelium resulted in heterogeneous glomeruli in ectopic VL olfactory bulb areas.

Different changes in cell division, apoptosis, and differentiation in Z1 versus Z4

The anomalous DM^{high}–VL^{low} expression gradient of AC3 in Cyp26B1 mice showed that Cyp26B1 inhibited OSNs differentiation in a graded manner that did not follow the Z1/Z2-4 division that NQO1 and NCAM2 expression demarcates (Fig. 4*A*). Neither did the epithelial Z1/Z2-4 division adequately correspond to the altered OR expression frequencies in the Cyp26B1 mice; for example, at PD14, Z2 OR expression was increased, Z3 OR expression was unchanged/decreased, and Z4 OR expression was decreased (Fig. 3*E*). Because of the overlap between OR expression zones and the graded manifestation of the phenotype, we focused our further analyses on cells located in olfactory epithelial areas in transgenic and control mice that corresponded to Z1 and Z4 (arrowheads in Fig. 1*A*). To address the decreased differentiation of OSNs in the VL olfactory epithelium further, we performed double SCG10/OMP immunohistochemical analysis. SCG10 is a protein that is selectively expressed in immature OSNs (Camoletto et al., 2001). $SCG10^+$ cells were increased in Z4 of PD5, PD14, and 6-month-old Cyp26B1 transgenic mice compared with control mice (Fig. 6*A*). No change in SCG10 immunoreactivity was apparent in Z1 of transgenic mice (Fig. 6*A*).

Quantification of epithelial areas with $SCG10^+$ OSNs in Z4 at PD14 indicated that the number of immature OSNs was increased 1.4-fold in Z4 of the transgenic mice (Fig. 6*B*, 3.0 ± 0.8 × $10^3/\mu m^2$ in control vs 4.5 ± 0.9 × $10^3/\mu m^2$ in transgenic mice, $p < 0.001$). At the same ages, the areas of OMP^+ OSNs in Z4 were similar in control and Cyp26B1 mice (Fig. 6*B*, 2.9 ± 0.5 × $10^3/\mu m^2$ in control vs 3.0 ± 0.8 × $10^3/\mu m^2$ in transgenic mice, $p = 0.6$). The number of OSNs that coexpressed SCG10 and OMP was increased 2.5-fold in transgenic mice (0.4 ± 0.1 cells/mm^2 in control vs 1.0 ± 0.2 cells/mm^2 in transgenic mice, $p < 0.001$). Quantification of $pH3^+$ cells and activated caspase-3^+ cells indicated that the proliferation and cell death in Z4 were increased 1.6- and 5.6-fold, respectively, in Cyp26B1 mice compared with control mice (Fig. 6*B*). The

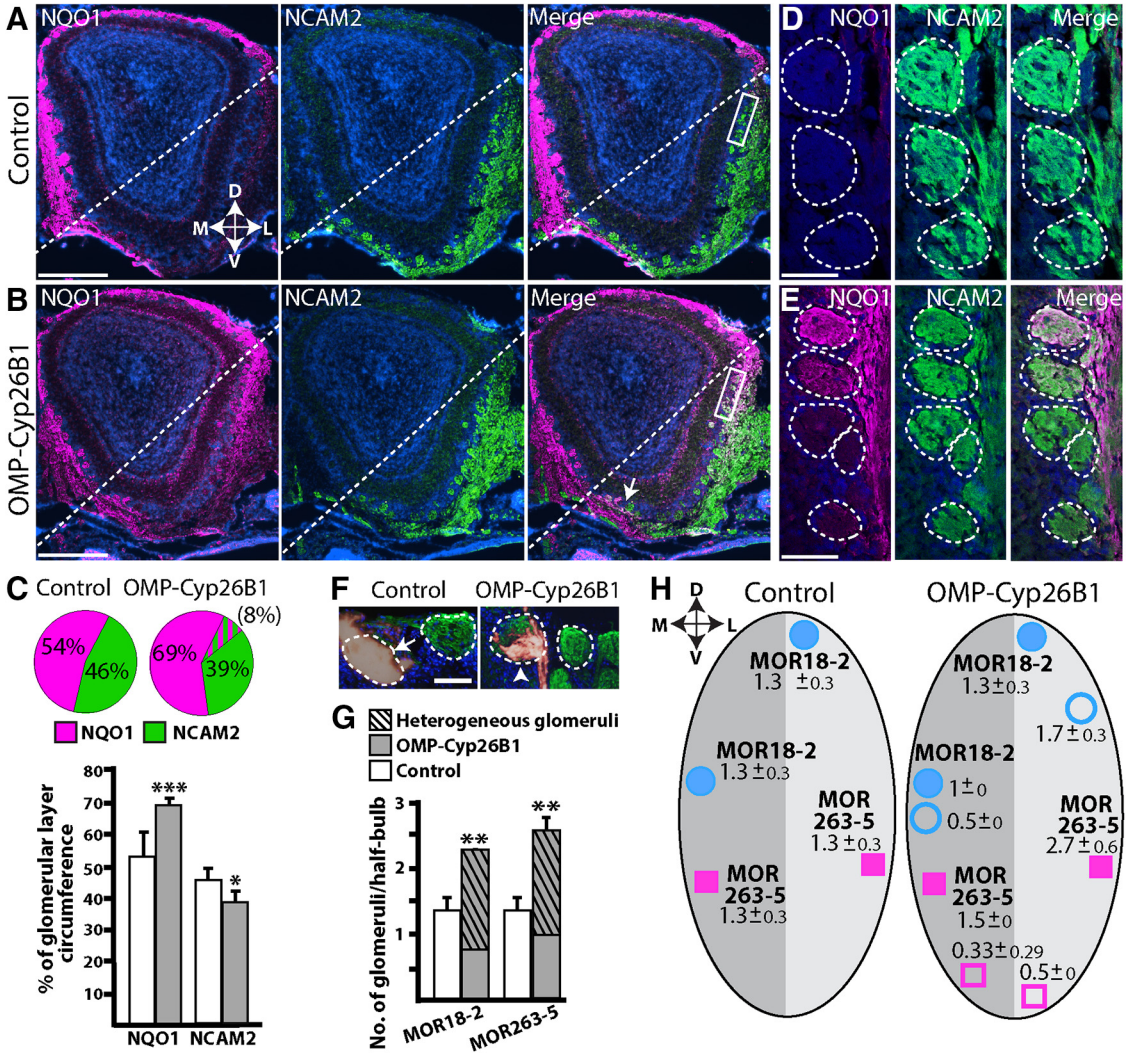

Figure 5. Transgenic overexpression of Cyp26B1 results in DM OSN axonal innervation into ectopic VL regions of the olfactory bulb glomerular layer. ***A***, ***B***, Representative images of double NQO1 (Z1, magenta) and NCAM2 (Z2-4, green) immunohistochemical analyses of consecutive sections of olfactory bulb of PD45 Cyp26B1 transgenic and littermate control mice. Dashed lines in ***A*** and ***B*** indicate the border between glomeruli formed by NCAM2$^+$ axons and NCAM2$^-$ axons. ***C***, Measurements of the linear length of NQO1$^+$ and NCAM2$^+$ glomerular regions relative to the circumference of the glomerular layer in PD45 OMP-Cyp26B1 (gray bars) and littermate control mice (open bars). The ratio of NQO1, NCAM2, and NQO1/NCAM2 overlap is indicated in the pie chart. ***D***, ***E***, Close ups of the areas boxed in (***A***, ***B***) showing NQO1$^-$/NCAM2$^+$ glomeruli in a control mouse (***D***) and glomeruli that are heterogeneous innervated by axons of both NQO1$^+$ and NCAM2$^+$ OSNs in a Cyp26B1 transgenic mouse (***E***). Dashed lines outline individual glomeruli. Indicated is a ventral olfactory bulb region that, like the boxed region in the dorsal olfactory bulb, has heterogeneous glomeruli (arrow in ***B***). ***F***, Double OMP immunohistochemical (green) and β-gal histochemical (yellow) analyses showing β-gal$^+$ MOR18-2 axons in a homogenous (arrow) and heterogeneous (arrowhead) MOR18-2 glomeruli. ***G***, Quantifications of MOR18-2 and MOR263-5 glomeruli in olfactory bulb of PD45 Cyp26B1 transgenic mice (gray bars) and littermate control mice (open bars). Striped bars indicate the number of heterogeneous glomeruli innervated by axons of >1 OR identity. ***H***, Schematic representation of the localizations and numbers of MOR18-2 (circles) and MOR263-5 (squares) glomeruli per half-bulb in PD45 control and transgenic Cyp26B1 mice. The different shades of gray indicate the two mirror-image maps of glomeruli in each olfactory bulb. Indicated are also invariant glomeruli (filled) and ventrally located ectopic glomeruli (open). All values represent mean and SD per hemisection ($n = 48$), *$p < 0.05$, **$p < 0.01$ ***$p < 0.001$, Student's *t* test, two tailed. Scale bars: ***A***, ***B***, 500 μm; ***D–F***, 50 μm.

numbers were; 5.5 ± 2.4 pH3$^+$ cells/mm in control versus 8.6 ± 3.2 pH3$^+$ cells/mm in transgenic mice ($p < 0.01$) and 0.4 ± 0.3 caspase3$^+$ cells/mm^2 in control versus 1.9 ± 0.6 caspase3$^+$ cells/mm^2 in transgenic mice ($p < 0.001$). The increased cell division and increased apoptosis indicated that the turnover of OSNs was increased in Z4, whereas the accumulation of SCG10$^+$ cells indicated that the differentiation into OMP$^+$ OSNs was inhibited in Z4.

Unlike the phenotype in Z4, the numbers of dividing pH3$^+$ cells in Z1 were similar in control and Cyp26B1 mice at PD14 (Fig. 6*B*, 6.8 ± 2.4 cells/mm in control vs 7.8 ± 3.6 in transgenic mice, $p = 0.4$). The expression of SCG10 increased marginally in Z1 (1.1-fold, i.e., 3.0 ± 0.5 × 10^3/μm^2 in control vs 3.4 ± 0.5 × 10^3/μm^2 in transgenic mice, $p < 0.05$), whereas the number of double SCG10/OMP$^+$ OSNs was unaltered in Z1 (0.2 ± 0.2 × 10^{-3} cells/μm^2 in control vs 0.2 ± 0.2 × 10^{-3} cells/μm^2 transgenic mice, $p = 0.75$). The number of activated caspase3$^+$ cells was increased 2-fold in Z1 (Fig. 6*B*, 0.9 ± 0.4 × 10^{-3} cells/μm^2 in control vs 1.9 ± 0.6 in transgenic mice, $p < 0.001$).

These results are consistent with a model in which increased RA degradation during the first postnatal weeks resulted in increased progenitor cell proliferation and inhibited OSN differentiation in Z4. In Z1, proliferation was unaffected and the effects on OSN differentiation and cell death were considerably less pronounced. However, at a later postnatal time point (PD45), the proliferation was increased also in Z1 of the transgenic mice (Fig. 4*D*).

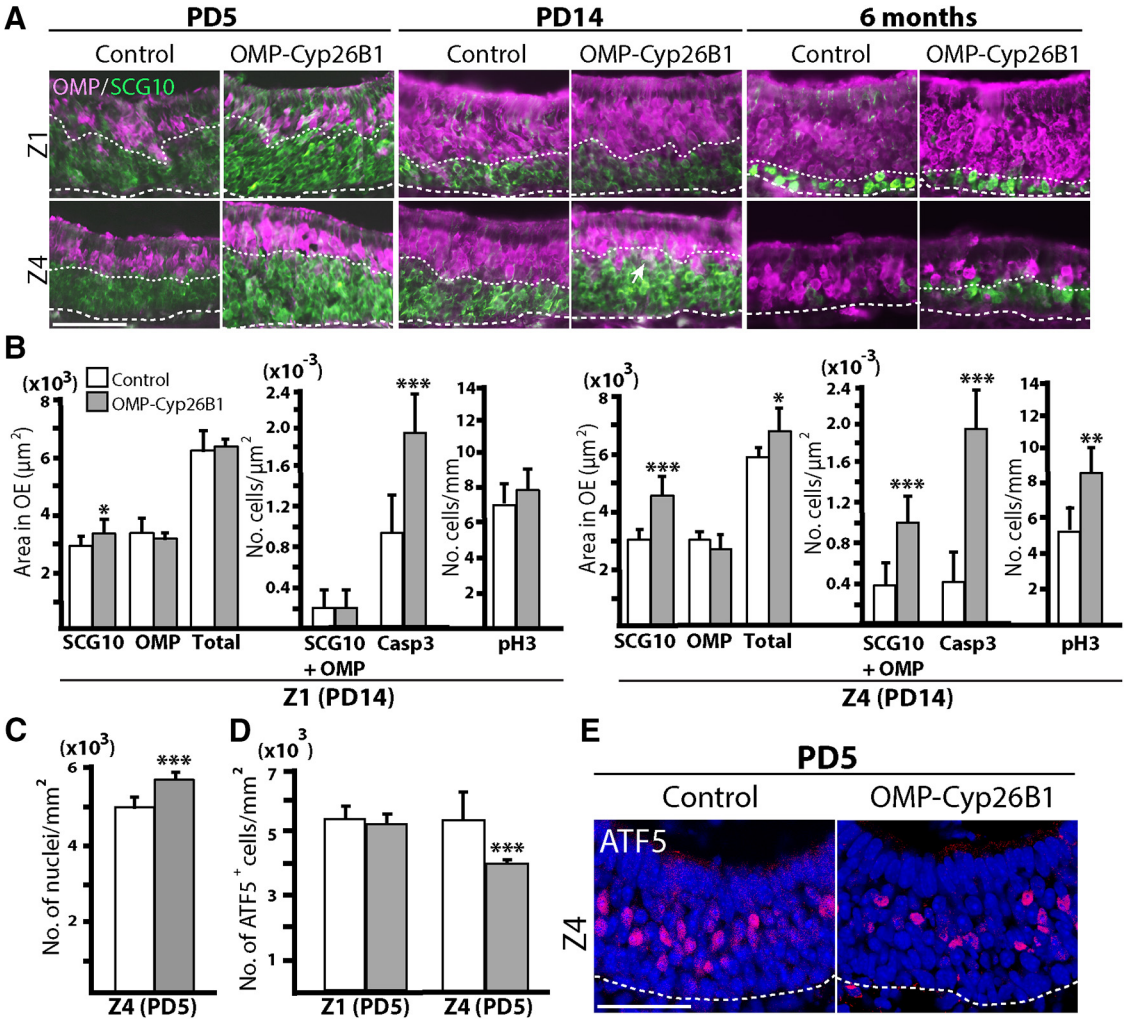

Figure 6. Cyp26B1 inhibits differentiation of Z4 OSNs at a stage before onset of OR expression ***A***, Double OMP (magenta) and SCG10 (green) immunohistochemical analyses of Z1 and Z4 in the olfactory epithelium of PD5, PD14, and 6-month-old Cyp26B1 transgenic and littermate control mice. ***B–D***, Quantifications of immunohistochemical analysis of Z1 and Z4 at PD14. Shown are OMP $^+$ and SCG10 $^+$ area sizes in Z1 and Z4 in Cyp26B1 transgenic (gray bars) and littermate control (open bars) mice. Shown are also quantifications, within the same areas, of number of cells that are immunoreactive for pH3 and activated caspase-3 (Casp3). ***C***, Total number Hoechst $^+$ nuclei located in the neuronal layer of Z4 at PD5 in Cyp26B1 transgenic (gray bars) and littermate control (open bars) mice. ***D***, Quantification of OSNs immunoreactive for ATF5 in Z1 and Z4 at PD5 in Cyp26B1 transgenic (gray bars) and littermate control (open bars) mice. ***E***, ATF5 (magenta) immunohistochemical analysis of olfactory epithelium of PD5 Cyp26B1 transgenic mice and littermate control mice. All values represent mean and SD; $n = 48$, $^{**}p < 0.01$, $^{***}p < 0.001$, Student's t test, two tailed. Scale bars in ***A*** and ***E***, 50 μm.

Differentiation of VL OSNs is decreased before onset of ATF5 and OR expression

An intriguing observation was that the expression of Z4 ORs (MOR235-1 and MOR244-1) decreased at PD14 even though the total number of OSNs in Z4 increased (Figs. 3*C*,*D*, 6*B*). To confirm this result, we quantified the total number of Hoechst $^+$ nuclei at PD5 in the neural cell layer of Z4 (Fig. 6*C*), which was a at a developmental time point when decreased expression of Z4 ORs first was evident (Fig. 3*F*). The total number of OSNs in Z4 of PD5 CypB26B1 mice was increased 12% relative to control mice (Fig. 6*D*). The increased number of Z4 OSNs at PD5 was consistent with our observation of increased cell division without concomitant increased cell death at this time point (Fig. 2*F*,*G*). One possibility that could explain the discrepancy between an increased number of Z4 OSNs and a decreased number of OSNs expressing Z4 ORs was ectopic expression of Z1-3 ORs in Z4. Arguing against this possibility were results showing that the expression patterns of Z1 and Z2 ORs did not ectopically expand into Z4 (data not shown) and that the numbers of OSNs expressing the Z3 ORs MOR256-17 and MOR256-55 were decreased and unaltered, respectively (Fig. 3*E*). Another, nonmutually exclusive explanation was that the transgenic mice had an increased number of immature SCG10 $^+$ Z4 OSNs that did not express any OR. The decreased expression of Z4 ORs correlated with reduced AC3 expression in Z4 (Fig. 4*A*,*C*). AC3 is part of the OR-mediated feedback mechanism that stabilizes OR choice and prevents OR switching (Dalton et al., 2013; Lyons et al., 2013). The first OR expressed in immature OSNs induces AC3 via selective translation of ATF5. AC3 expression subsequently stabilizes OR gene switching such that one OR gene per OSN become stably expressed at a very high level. To address directly whether Cyp26B1 influenced ATF5 expression in Z1 and Z4 differently, we quantified the number of ATF5-immunopositive OSNs at PD5. The number of ATF5 $^+$ OSNs was decreased in Z4, but not in Z1, of Cyp26B1 mice (Fig. 6*D*,*E*). ATF5 numbers in Z1 of control mice and transgenic mice were 5.4 $\pm$ 0.5 and 5.1 $\pm$ 0.3 ATF5 $^+$ cells/mm ^{2}, respectively ($p = 0.33$). The corresponding numbers in Z4 of control mice and transgenic mice were 5.2 $\pm$ 1.2 and 3.9 $\pm$ 0.7

ATF5$^+$ cells/mm^2, respectively ($p < 0.001$). Collectively, these results indicated that Cyp26B1 inhibited differentiation of SCG10$^+$ OSNs at a stage before onset of ATF5, AC3, and OR expression. Moreover, the results suggested that VL OSNs are more vulnerable to the effect of reduced RA concentrations, which is consistent with the fact that VL OSNs under normal circumstances express low levels of Cyp26B1 and are surrounded by cells that express high levels of RALDH enzymes.

Discussion

Diversification of sensory cell classes ensures optimal detection of external world stimuli, whereas neuroplasticity allows the organism to respond and adapt to changes in the environment. This fact is exemplified in the olfactory epithelium by stimulus-driven changes in the relative abundance of different OR-specific classes of OSNs (Santoro and Dulac, 2012; Zhao et al., 2013). Here, we have addressed the hypothesis that the normally dynamic and spatially graded Cyp26B1 expression is one mechanism by which stimulus-dependent activity modulates the OR repertoire. To this end, we have analyzed transgenic mice in which the Cyp26B1 level is made constant in OSNs throughout the DM–VL extent of the olfactory epithelium. Interestingly, the initial phenotypic effects during the first postnatal week are specific to the VL epithelium. In addition to increased VL progenitor cell proliferation, we find that Cyp26B1 significantly decreases OSN differentiation at a stage before onset of OR expression. The increased proliferation and decreased OSN differentiation initially occur in the absence of enhanced cell death and therefore the result is an accumulation of immature OSNs. We found the number of OSNs expressing ATF5 to be reduced. ATF5 is a transcription factor that induces AC3 expression, which in turn promotes stabilization of OR gene choice and high steady-state levels of OR expression (Dalton et al., 2013). It is thus conceivable that the reduced expression of VL ORs observed is a consequence of inhibited OSN differentiation and accumulation of "empty" OSNs that do not express any OR to a high level. AC3 expression turns into a DM^{high}–VL^{low} gradient in Cyp26B1 mice. These results indicate that the effect of increased RA degradation by Cyp26B1 influences OSN differentiation and onset of OR expression in a graded manner, as opposed to a threshold or zone-specific manner. The results also reveal that RA presence is necessary for the normal postnatal patterns of the olfactory epithelium because Cyp26B1 mice show a novel phenotype of DM expansion at the expense of VL olfactory epithelial and olfactory bulb territories.

Conceivably, the stimulation of progenitor cell division observed is mediated by a non-cell-autonomous Cyp26B1 function because the promotor driving Cyp26B1 expression in the transgenic mice is inactive in progenitor cells. A plausible mechanism is that Cyp26B1 acts as a "sink" for diffusible RA produced by RALDH3$^+$ cells in the absolute vicinity of dividing progenitor cells in the VL epithelium. Such a model is consistent with the observed increased progenitor cell proliferation in the olfactory epithelium of vitamin A deficient rats, as well as in the olfactory epithelium of mouse embryos deficient in RALDH3 (Asson-Batres et al., 2003b; Paschaki et al., 2013). Moreover, the fact that OSN progenitor cells normally express high levels of CRABP2 (Asson-Batres et al., 2003a), which binds diffusible RA and delivers it to nuclear RARs in a recipient cell, is also compatible with this model.

A remarkable finding is that the constitutive presence of Cyp26B1 influences expression frequencies of individual OR genes in the DM and the VL olfactory epithelium differently. Therefore, in contrast to the decreased or unaltered Z3-4 OR expression in the VL epithelium, the frequencies of Z1-2 ORs in the DM epithelium are increased or unaltered. Analysis with a general Z1 OSN marker, NQO1, shows that the extent of Z1 olfactory epithelium increases and analysis of the olfactory bulb demonstrates a broaden innervation of Z1 OSN axon terminals into more ventrally located glomeruli, which in control mice are formed exclusively by Z2-4 axon terminals. Moreover, the use of Z1 and Z2 OR-specific reporter mice show that the increased frequencies of specific ORs in the Cyp26B1 mice correlate with the formation of supernumerary glomeruli for the specific ORs, as well as a broadened innervation of axons into ectopic ventrally located glomeruli. In the olfactory epithelium all zones except Z4 expand ventrolaterally. Together, these results show that that a constitutive, increased, and nongraded Cyp26B1 expression during the first postnatal month results in a DM expansion of OR zones and glomerular target areas in the olfactory epithelium and bulb, respectively. The postnatal DM expansion most likely is a consequence of OSNs that, depending on their location along the DM–VL axis, gradually become more sensitive to the reduction in the extracellular RA concentration. The more ventrolaterally located they are, the greater the tendency of newly generated OSNs to be inhibited in differentiation at a stage before OR and AC3 expression, which in turn decreases cell survival, negatively affecting the target selection and formation of homogeneous glomeruli with stable connections in the bulb. DM OSNs are relatively less sensitive to reduced RA concentration and therefore prevail over more ventrolaterally located OSNs, which are more sensitive to reduced RA concentration. Moreover, Z4, the most ventrolaterally located OSNs, is affected most.

It is known that sensory deprivation by unilateral naris occlusion inhibits OSN turnover and alters OR expression frequencies (Zou et al., 2004; Kikuta et al., 2015). Interestingly, sensory deprivation causes expression frequencies of VL ORs to increase or be unaltered, whereas the frequencies of DM OR decrease or are unaltered (Zhao et al., 2013). This inverse relationship between the effects of sensory deprivation and degradation of RA by Cyp26B1 on both OSN turnover and zone-specific OR frequencies is causally related to the fact that sensory deprivation inhibits Cyp26B1 expression in OSNs (Öztokatli et al., 2012; Login et al., 2015). However, not all ORs that we analyzed were inversely regulated by Cyp26B1 and sensory deprivation (e.g., MOR244-1 and MOR256-55, this study; Zhao et al., 2013). Moreover, naris occlusion appears to affect OR frequencies differently also along the anterior–posterior axis of the olfactory epithelium (Santoro and Dulac, 2012). These differences are conceivably consequences of the fact that sensory stimulation influences several other gene-regulatory pathways in addition to RA signaling (Spehr et al., 2002; Watt et al., 2004; Santoro and Dulac, 2012; Colquitt et al., 2014; Kim et al., 2015). Activity-dependent Cyp26B1 expression is therefore most likely one mechanism of a limited number of distinct mechanisms that work in concert to modify OR expression frequencies in response to environmental changes. Another mechanism that has a direct impact on the lifespan of OSNs and OR expression frequencies is the stimulus-dependent downregulation of the OSN-specific histone variant H2BE (Santoro and Dulac, 2012). Although the normal expression of Cyp26B1, in contrast to H2BE, is graded and requires a functional CNG channel, it is interesting that changes in OR frequencies after sensory deprivation are significantly reduced in H2BE-deficient mice (Öztokatli et al., 2012; Santoro and Dulac, 2012; Login et al., 2015).

Recent studies indicate that activation of some OSNs in the DM olfactory epithelium can elicit innate behaviors (Kobay-

akawa et al., 2007; Cho et al., 2011; Ferrero et al., 2011; Dewan et al., 2013; Matsuo et al., 2015). One feature of the VL epithelium is that the turnover of OSNs is relatively high (Vedin et al., 2009). Therefore, the DM olfactory epithelium appears to promote OSNs to form stable, if not "hardwired," connections, whereas the VL epithelium exhibits characteristics that allow for a high degree of neurogenic plasticity that may facilitate both adaptive and learned behaviors. One physiological function of stimulus-dependent and graded Cyp26B1 may thus be to support the maintenance of the integrity of connectivity of OSNs that mediate innate behaviors by negatively influencing differentiation of relatively more VL located OSNs. The non-cell-autonomous stimulation of neurogenesis by increased Cyp26B1 also suggests the interesting possibility that increased Cyp26B1 activity in response to odors that mediate innate behaviors through stimulation of the DM region promotes adaptive and/or learning-dependent neurogenic plasticity in relatively more VL parts.

RALDHs and/or Cyp26Bs regulating functional diversity within a topographically organized network of neural connections is not limited to the olfactory sensory map. Region-specific RALDH and Cyp26B1 expression underlie differential neurogenicity in populations of adult spinal cord progenitor cells during development (Leung et al., 2012), as well as spatial differences in hippocampal neurogenesis in adult mice (Goodman et al., 2012). Spatially patterned expression of RALDHs and Cyp26s have also been shown to determine tonotopically patterned hair cells in chicken cochlea (Thiede et al., 2014) and are suggested to contribute in forming retinal specializations for higher acuity vision in mammals (Luo et al., 2006). Whether activity-dependent Cyp26B1 expression modifies connectivity within these systems by a mechanism similar to that suggested in the present study is an interesting question for future investigations.

References

Alenius M, Bohm S (1997) Identification of a novel neural cell adhesion molecule-related gene with a potential role in selective axonal projection. J Biol Chem 272:26083–26086. CrossRef Medline

Alenius M, Bohm S (2003) Differential function of RNCAM isoforms in precise target selection of olfactory sensory neurons. Development 130: 917–927. CrossRef Medline

Asson-Batres MA, Smith WB (2006) Localization of retinaldehyde dehydrogenases and retinoid binding proteins to sustentacular cells, glia, Bowman's gland cells, and stroma: potential sites of retinoic acid synthesis in the postnatal rat olfactory organ. J Comp Neurol 496:149–171. CrossRef Medline

Asson-Batres MA, Ahmad O, Smith WB (2003a) Expression of the cellular retinoic acid binding proteins, type II and type I, in mature rat olfactory epithelium. Cell Tissue Res 312:9–19. Medline

Asson-Batres MA, Zeng MS, Savchenko V, Aderoju A, McKanna J (2003b) Vitamin A deficiency leads to increased cell proliferation in olfactory epithelium of mature rats. J Neurobiol 54:539–554. CrossRef Medline

Astic L, Saucier D (1986) Anatomical mapping of the neuroepithelial projection to the olfactory bulb in the rat. Brain Res Bull 16:445–454. CrossRef Medline

Buck L, Axel R (1991) A novel multigene family may encode odorant receptors: a molecular basis for odor recognition. Cell 65:175–187. CrossRef Medline

Camoletto P, Colesanti A, Ozon S, Sobel A, Fasolo A (2001) Expression of stathmin and SCG10 proteins in the olfactory neurogenesis during development and after lesion in the adulthood. Brain Res Bull 54:19–28. CrossRef Medline

Cho JH, Prince JE, Cutforth T, Cloutier JF (2011) The pattern of glomerular map formation defines responsiveness to aversive odorants in mice. J Neurosci 31:7920–7926. CrossRef Medline

Colquitt BM, Markenscoff-Papadimitriou E, Duffié R, Lomvardas S (2014) Dnmt3a regulates global gene expression in olfactory sensory neurons and enables odorant-induced transcription. Neuron 83:823–838. CrossRef Medline

Conzelmann S, Levai O, Bode B, Eisel U, Raming K, Breer H, Strotmann J (2000) A novel brain receptor is expressed in a distinct population of olfactory sensory neurons. Eur J Neurosci 12:3926–3934. CrossRef Medline

Dalton RP, Lyons DB, Lomvardas S (2013) Co-opting the unfolded protein response to elicit olfactory receptor feedback. Cell 155:321–332. CrossRef Medline

Dewan A, Pacifico R, Zhan R, Rinberg D, Bozza T (2013) Non-redundant coding of aversive odours in the main olfactory pathway. Nature 497: 486–489. CrossRef Medline

Dias BG, Ressler KJ (2014) Parental olfactory experience influences behavior and neural structure in subsequent generations. Nat Neurosci 17: 89–96. Medline

Ferrero DM, Lemon JK, Fluegge D, Pashkovski SL, Korzan WJ, Datta SR, Spehr M, Fendt M, Liberles SD (2011) Detection and avoidance of a carnivore odor by prey. Proc Natl Acad Sci U S A 108:11235–11240. CrossRef Medline

Goodman T, Crandall JE, Nanescu SE, Quadro L, Shearer K, Ross A, McCaffery P (2012) Patterning of retinoic acid signaling and cell proliferation in the hippocampus. Hippocampus 22:2171–2183. CrossRef Medline

Gussing F, Bohm S (2004) NQO1 activity in the main and the accessory olfactory systems correlates with the zonal topography of projection maps. Eur J Neurosci 19:2511–2518. CrossRef Medline

Hägglund M, Berghard A, Strotmann J, Bohm S (2006) Retinoic acid receptor-dependent survival of olfactory sensory neurons in postnatal and adult mice. J Neurosci 26:3281–3291. CrossRef Medline

Hirota J, Omura M, Mombaerts P (2007) Differential impact of Lhx2 deficiency on expression of class I and class II odorant receptor genes in mouse. Mol Cell Neurosci 34:679–688. CrossRef Medline

Ishii T, Omura M, Mombaerts P (2004) Protocols for two- and three-color fluorescent RNA in situ hybridization of the main and accessory olfactory epithelia in mouse. J Neurocytol 33:657–669. CrossRef Medline

Jones SV, Choi DC, Davis M, Ressler KJ (2008) Learning-dependent structural plasticity in the adult olfactory pathway. J Neurosci 28:13106–13111. CrossRef Medline

Kaluza JF, Gussing F, Bohm S, Breer H, Strotmann J (2004) Olfactory receptors in the mouse septal organ. J Neurosci Res 76:442–452. CrossRef Medline

Kikuta S, Sakamoto T, Nagayama S, Kanaya K, Kinoshita M, Kondo K, Tsunoda K, Mori K, Yamasoba T (2015) Sensory deprivation disrupts homeostatic regeneration of newly generated olfactory sensory neurons after injury in adult mice. J Neurosci 35:2657–2673. CrossRef Medline

Kim SY, Yoo SJ, Ronnett GV, Kim EK, Moon C (2015) Odorant stimulation promotes survival of rodent olfactory receptor neurons via PI3K/Akt activation and Bcl-2 expression. Mol Cells 38:535–539. CrossRef Medline

Kobayakawa K, Kobayakawa R, Matsumoto H, Oka Y, Imai T, Ikawa M, Okabe M, Ikeda T, Itohara S, Kikusui T, Mori K, Sakano H (2007) Innate versus learned odour processing in the mouse olfactory bulb. Nature 450:503–508. CrossRef Medline

LaMantia AS, Bhasin N, Rhodes K, Heemskerk J (2000) Mesenchymal/epithelial induction mediates olfactory pathway formation. Neuron 28:411–425. CrossRef Medline

Leung C, Chan SC, Tsang SL, Wu W, Sham MH (2012) Cyp26b1 mediates differential neurogenicity in axial-specific populations of adult spinal cord progenitor cells. Stem Cells Dev 21:2252–2261. CrossRef Medline

Li Q, Korzan WJ, Ferrero DM, Chang RB, Roy DS, Buchi M, Lemon JK, Kaur AW, Stowers L, Fendt M, Liberles SD (2013) Synchronous evolution of an odor biosynthesis pathway and behavioral response. Curr Biol 23: 11–20. Medline

Login H, Butowt R, Bohm S (2015) Activity-dependent and graded BACE1 expression in the olfactory epithelium is mediated by the retinoic acid metabolizing enzyme CYP26B1. Brain Struct Funct 220:2143–2157. CrossRef Medline

Luo T, Sakai Y, Wagner E, Dräger UC (2006) Retinoids, eye development, and maturation of visual function. J Neurobiol 66:677–686. CrossRef Medline

Lyons DB, Allen WE, Goh T, Tsai L, Barnea G, Lomvardas S (2013) An epigenetic trap stabilizes singular olfactory receptor expression. Cell 154: 325–336. CrossRef Medline

Matsuo T, Hattori T, Asaba A, Inoue N, Kanomata N, Kikusui T, Kobayakawa R, Kobayakawa K (2015) Genetic dissection of pheromone processing reveals main olfactory system-mediated social behaviors in mice. Proc Natl Acad Sci U S A 112:E311–E320. CrossRef Medline

Miyamichi K, Serizawa S, Kimura HM, Sakano H (2005) Continuous and overlapping expression domains of odorant receptor genes in the olfactory epithelium determine the dorsal/ventral positioning of glomeruli in the olfactory bulb. J Neurosci 25:3586–3592. CrossRef Medline

Mombaerts P, Wang F, Dulac C, Chao SK, Nemes A, Mendelsohn M, Edmondson J, Axel R (1996) Visualizing an olfactory sensory map. Cell 87:675–686. CrossRef Medline

Niederreither K, McCaffery P, Dräger UC, Chambon P, Dolle P (1997) Restricted expression and retinoic acid-induced downregulation of the retinaldehyde dehydrogenase type 2 (RALDH-2) gene during mouse development. Mech Dev 62:67–78. CrossRef Medline

Niederreither K, Fraulob V, Garnier JM, Chambon P, Dollé P (2002) Differential expression of retinoic acid-synthesizing (RALDH) enzymes during fetal development and organ differentiation in the mouse. Mech Dev 110:165–171. CrossRef Medline

Nishizumi H, Sakano H (2015) Developmental regulation of neural map formation in the mouse olfactory system. Dev Neurobiol 75:594–607. CrossRef Medline

Norlin EM, Alenius M, Gussing F, Hägglund M, Vedin V, Bohm S (2001) Evidence for gradients of gene expression correlating with zonal topography of the olfactory sensory map. Mol Cell Neurosci 18:283–295. CrossRef Medline

Öztokatli H, Hörnberg M, Berghard A, Bohm S (2012) Retinoic acid receptor and CNGA2 channel signaling are part of a regulatory feedback loop controlling axonal convergence and survival of olfactory sensory neurons. FASEB J 26:617–627. CrossRef Medline

Paschaki M, Cammas L, Muta Y, Matsuoka Y, Mak SS, Rataj-Baniowska M, Fraulob V, Dollé P, Ladher RK (2013) Retinoic acid regulates olfactory progenitor cell fate and differentiation. Neural Dev 8:13. CrossRef Medline

Peluso CE, Jang W, Dräger UC, Schwob JE (2012) Differential expression of components of the retinoic acid signaling pathway in the adult mouse olfactory epithelium. J Comp Neurol 520:3707–3726. CrossRef Medline

Ressler KJ, Sullivan SL, Buck LB (1994) Information coding in the olfactory system: evidence for a stereotyped and highly organized epitope map in the olfactory bulb. Cell 79:1245–1255. CrossRef Medline

Ross AC, Zolfaghari R (2011) Cytochrome P450s in the regulation of cellular retinoic acid metabolism. Annu Rev Nutr 31:65–87. CrossRef Medline

Santoro SW, Dulac C (2012) The activity-dependent histone variant H2BE modulates the life span of olfactory neurons. Elife 1:e00070. CrossRef Medline

Saucier D, Astic L (1986) Analysis of the topographical organization of olfactory epithelium projections in the rat. Brain Res Bull 16:455–462. CrossRef Medline

Spehr M, Wetzel CH, Hatt H, Ache BW (2002) 3-phosphoinositides modulate cyclic nucleotide signaling in olfactory receptor neurons. Neuron 33:731–739. CrossRef Medline

Thiede BR, Mann ZF, Chang W, Ku YC, Son YK, Lovett M, Kelley MW, Corwin JT (2014) Retinoic acid signalling regulates the development of tonotopically patterned hair cells in the chicken cochlea. Nat Commun 5:3840. Medline

Vassar R, Chao SK, Sitcheran R, Nuñez JM, Vosshall LB, Axel R (1994) Topographic organization of sensory projections to the olfactory bulb. Cell 79:981–991. CrossRef Medline

Vedin V, Molander M, Bohm S, Berghard A (2009) Regional differences in olfactory epithelial homeostasis in the adult mouse. J Comp Neurol 513:375–384. CrossRef Medline

Watt WC, Sakano H, Lee ZY, Reusch JE, Trinh K, Storm DR (2004) Odorant stimulation enhances survival of olfactory sensory neurons via MAPK and CREB. Neuron 41:955–967. CrossRef Medline

Whitesides J, Hall M, Anchan R, LaMantia AS (1998) Retinoid signaling distinguishes a subpopulation of olfactory receptor neurons in the developing and adult mouse. J Comp Neurol 394:445–461. Medline

Yoshihara Y, Kawasaki M, Tamada A, Fujita H, Hayashi H, Kagamiyama H, Mori K (1997) OCAM: a new member of the neural cell adhesion molecule family related to zone-to-zone projection of olfactory and vomeronasal axons. J Neurosci 17:5830–5842. Medline

Zhao S, Tian H, Ma L, Yuan Y, Yu CR, Ma M (2013) Activity-dependent modulation of odorant receptor gene expression in the mouse olfactory epithelium. PLoS One 8:e69862. CrossRef Medline

Zou DJ, Feinstein P, Rivers AL, Mathews GA, Kim A, Greer CA, Mombaerts P, Firestein S (2004) Postnatal refinement of peripheral olfactory projections. Science 304:1976–1979. CrossRef Medline